Transmission electron microscopy, electron diffraction and hardness studies of high-pressure and high-temperature treated C_{60}

2000 J. Phys.: Condens. Matter 12 10411

(http://iopscience.iop.org/0953-8984/12/50/304)

J. Phys.: Condens. Matter **12** (2000) 10411–10421. Printed in the UK PII: S0953-8984(00)16039-4

Transmission electron microscopy, electron diffraction and hardness studies of high-pressure and high-temperature treated C_{60}

R A Wood†, M H Lewis†, G West†, S M Bennington‡, M G Cain§ and N Kitamura‖

† Centre for Advanced Materials, Department of Physics, University of Warwick, Coventry CV4 7AL, UK
‡ ISIS Facility, Rutherford Appleton Laboratory, Chilton, Didcot, Oxfordshire OX11 0QX, UK
§ National Physical Laboratory, Queens Road, Teddington, Middlesex TW11 0LW, UK
‖ Osaka National Research Institute, Ikeda, Osaka, 563-8577, Japan

Received 2 August 2000, in final form 2 November 2000

Abstract. TEM and electron diffraction investigations were performed on high-temperature and high-pressure treated polymeric C_{60} fullerene, prepared at 700, 773 and 800 K in the pressure range of 3–9 GPa, for one hour. A mixed phase of alternating rhombohedral lamellae and tetragonal domains is formed, even at high pressures, with the ratio of polymers being dependent on the pressure applied. At higher temperatures, 900–1173 K, and for a similar pressure range, graphitic 'hard' carbon phases formed, via an interpolymer interface instability and/or shear mechanism. This phase exhibited a hardness of 10–15 GPa and a high degree of elastic recovery under indentation. Treatment times of 0.5–30 minutes for the graphitic phase showed the kinetics of graphitization to be slow (∼1 h) and proceeding via cross-linked intermediates containing trapped whole C_{60} cages. The influence of the cross-linking resulted in hardness values up to 33.5 GPa, for a twenty-minute treatment.

1. Introduction

Fullerene C_{60} was originally discovered in the middle of the 1980s [1] and initial interest was high. This however tapered off, until Kratschmer *et al* [2] discovered a facile and economically viable synthesis route. With the advent of affordable fullerenes, research resulted in the discovery of 1-D and 2-D polymers [3], synthesized as phototransformed thin film. The polymer formation is through a [2 + 2] cycloaddition of two adjacent '66' bonds, producing a four-membered sp^3 covalently bonded ring bridging two C_{60} molecules [4]. Bulk samples of these polymers were realized by exposing these fullerenes to high-temperature and high-pressure (HTHP) treatments [5–8]. This produced many new phases; at higher temperatures disordered sp^2 carbon [9–13] is formed and with increasing pressure it is reported to form 3-D polymeric structures [14, 15] and a second disordered phase containing mainly sp^3 carbons.

The pressure–temperature (P/T) diagram for C_{60} contains a host of crystalline, polymeric and disordered structures. These structures exhibit highly differing physical properties; the hardness values for polymeric phases are reported to be 1–2 GPa [11], whereas 3-D polymerics have a reported hardness of about 100 GPa. At slightly elevated temperatures, thermally activated polymerization occurs resulting in the formation of 1-D polymers, known as the orthorhombic phase. With increasing temperature the C_{60} chains have enough thermal energy

0953-8984/00/5010411+11$30.00

to form additional intermolecular covalent bonds resulting in the formation of two possible 2-D polymeric structures, tetragonal and rhombohedral [7–10]. The ratio of polymers attained depends mainly on the P/T regime used and whether pressure or temperature is applied first [8].

A simplified form of P/T phase diagram, constructed using recently published data, is presented in figure 1. A general trend with increase in temperature is the collapse of the C_{60} molecular cages to produce a predominantly sp^2 bonded graphitic 'hard' carbon [9, 12], which is considerably harder than the polymeric phase. At very high pressures, there is a rapid decrease in unit-cell volume, which indicates the formation of cubic 3-D polymers. In this region of the P/T diagram, increasing temperature results in a gradual increase in hardness, accompanying the reduction in the lattice constant, which may be attributed to the continuous formation of intermolecular bonds.

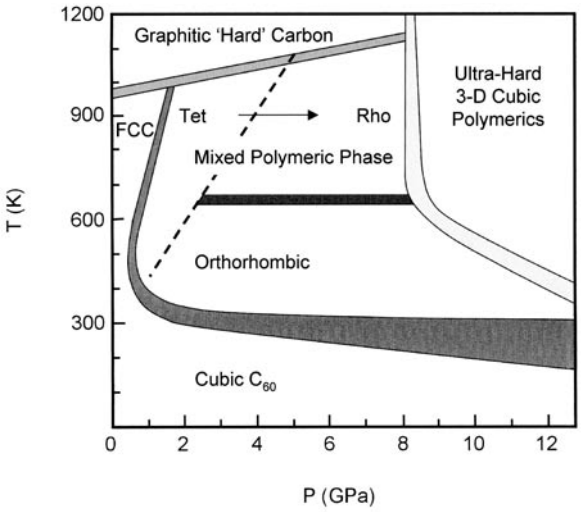

Figure 1. The pressure–temperature phase diagram for C_{60} fullerene.

It is still not conclusively proven whether some of the states observed in specimens rapidly cooled from the specific P/T conditions are intermediate, equilibrium states or combinations of several states. However, a recent '*in situ*' x-ray diffraction study confirms some elements of the P/T diagram [16]. Another factor that may influence phase boundaries or transformation kinetics is the occurrence of non-hydrostatic pressure in the preparation die, i.e. the proportion of shear stress, which may promote polymerization via relative translation of molecules or induce molecular collapse following the severance of polymerized bonds.

The research described in this paper attempts to understand some of the morphological features and mechanisms involved in transformations within the P–T field, using combined electron imaging and diffraction. The transformation to graphitic 'hard' carbons has also been studied with a view to identifying the origin of the time and P/T dependence of true hardness values, using depth-sensing nano-hardness probes.

2. Experimental procedure

2.1. Thermobaric treatments and XRD

The high-pressure and high-temperature treated fullerene samples were produced at the Osaka National Research Institute. The initial sample was 99.9% purity C_{60} purchased from the Materials and Electrochemical Research (MER) Corporation. The thermobaric conditions

were achieved using an octupole press. Pressure was applied, before subsequent heating and holding for periods ranging from half a minute to an hour. Samples were produced at temperatures of 773, 900, 973 and 1173 K with variations in pressure from 3 to 9 GPa. The rate of change of temperature during heating was 30 °C min^{-1} and the samples were quenched at approximately 200 °C s^{-1}. X-ray diffraction patterns were recorded from the quenched samples using Cu Kα radiation.

2.2. Indentation experiments

Hardness and elastic modulus measurements were carried out using a depth-sensing micro-indentation system within a SEM. This is able to take into account the elastic recovery exhibited by the sample, which is not allowed for with traditional indenting devices. The specimens were encapsulated in Bakelite cylinders, then polished prior to testing. For each sample ten separate indentations were performed using a load of 1000 mN, except for the softer 773 K preparations where a lower load of 250 mN was used.

2.3. TEM

The TEM sample preparation was performed on diamond-cut sections, lapped to $\sim$50 μm, before ion beam thinning to electron transparency in a Gatan PIPS system using an incident beam angle of $\sim$10° from the specimen surface. The thinned samples were imaged using a JEOL 2000FX TEM and selected-area diffraction used to identify phases with specific morphology.

3. Results and discussion

3.1. 2-D polymers

These phases are produced at temperatures ranging from 650 to 900 K and pressures up to approximately 10 GPa. The XRD spectra (figure 2) exemplify the evolution of the different polymers at 773 K over a pressure range of 3–9 GPa. With the application of thermobaric conditions the low-angle $(111)_C$ cubic reflection splits into the $\{101\}_T$ and $(110)_T$ ones and this is accompanied by the appearance of $(112)_T$ and $\{200\}_T$ ones, indicating the occurrence of polymerization. At 3 GPa the XRD trace could be indexed almost solely on the basis of the tetragonal phase; the only indications of the rhombohedral phase were weak shoulders at $\sim$11° and $\sim$13° associated with the $(00.3)_R$ and $(01.2)_R$ reflections. As the treatment pressure is increased to 6 GPa the rhombohedral phase becomes more obvious and conversely the tetragonal phase becomes weaker. The $(00.3)_R$ peak is now of approximately the same intensity as the $\{101\}_T$ and $(002)_T$ peaks. This evolution continues to 9 GPa where the tetragonal peaks have almost disappeared and the rhombohedral spectrum is now clearly visible, indicated by the domination of the $(10.4)_R$ peak over the $(112)_T$ peak. Therefore, it is evident that the proportion of rhombohedral phase produced is related to the magnitude of the pressure used. This could be due to the formation of the higher-density rhombohedral phase under pressure compared to a less dense tetragonal arrangement coupled to the influence of fcc crystal shear, with increased slip band density at high pressures.

Novel TEM investigations of the 2-D polymer samples prepared at 773 K, 3–9 GPa all exhibited regular bands of contrast, which ran in three distinct directions (figure 3(a)). Also, the concentration of these bands increases with treatment pressure. On varying the orientation of the sample it was noticeable that only two directions could be clearly visible at any one time. The two visible bands intersect at an angle of approximately 70° indicating that a transformation

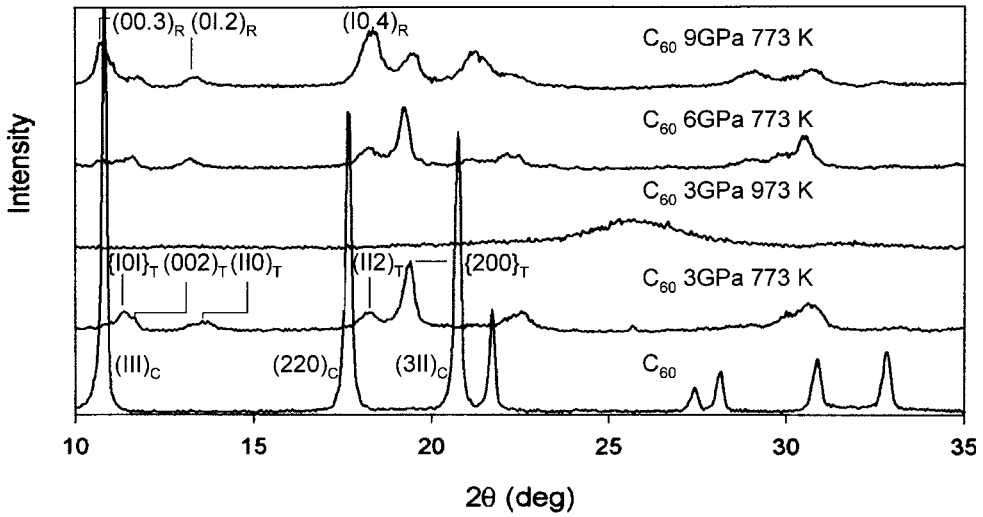

Figure 2. XRD traces illustrating the development of the polymeric phases with increase in pressure.

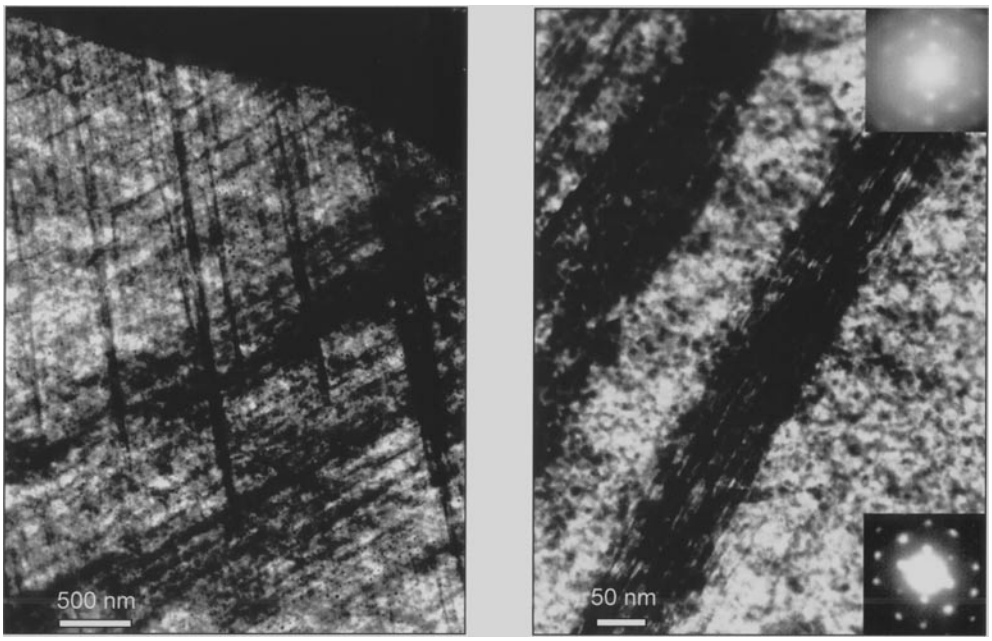

(a) (b)

Figure 3. TEM images of the (a) mixed polymeric phase and (b) rhombohedral lamellae.

has occurred parallel to the original $(111)_C$ planes, confirmed by electron diffraction of the polymer states.

In figure 3(b) the electron diffraction pattern from the lighter mottled area, shown in the bottom right-hand corner of the image, could be indexed as a body-centred tetragonal phase

with a $\langle 010\rangle_T$ electron beam direction (figure 4(a)). The diffraction aperture was then moved over the contrasting areas without a change in sample orientation. The diffraction pattern taken from this area bore a similarity to the previous pattern, but subtle distortions were noticeable. An indication of this is the angle between $(002)_T$ and $(200)_T$ changing from 90° to 95° for the equivalent $(01.2)_R$ and $(0\bar{1}.4)_R$ planes. The pattern was subsequently indexed as the rhombohedral polymeric phase, with a $[2\bar{1}.0]_R$ beam direction (figure 4(b)). Therefore, it can be inferred that rhombohedral lamellar domains have formed along planes parallel to the original $(111)_C$ planes. The relative orientations of the rhombohedral and tetragonal domains and the parent fcc phase are shown in figure 5, with the two $[0\bar{1}0]_T$ and $[21.0]_R$ beam directions being parallel and stemming from $[1\bar{1}0]_C$.

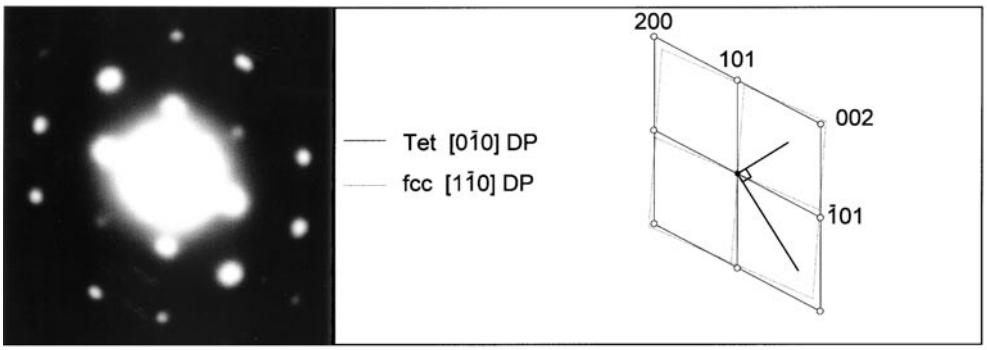

(a)

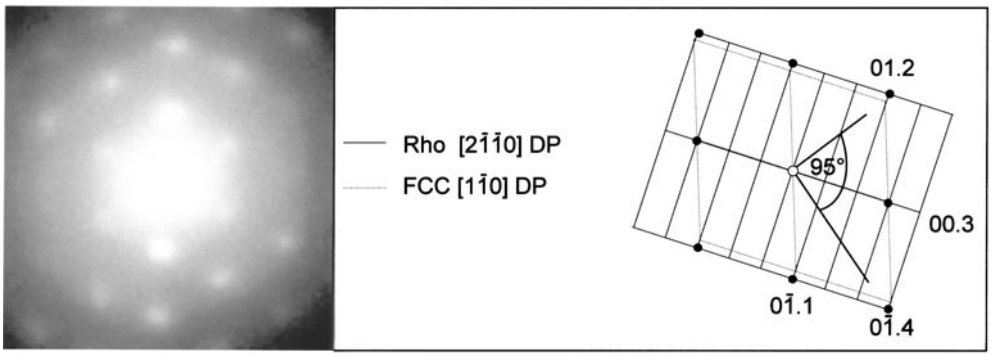

(b)

Figure 4. (a) The electron diffraction pattern indexed on a $[0\bar{1}0]_T$ beam direction. (b) The electron diffraction pattern indexed on a $[2\bar{1}\bar{1}0]_R$ beam direction.

The formation of microscopic domains in different variants of the rhombohedral orientation occurs to minimize internal stresses produced in the sample due to the rhombohedral or tetragonal lattice deformations. The original fcc C_{60} 'domains' correspond to the grain size in the as-received fullerene (10–100 μm) such that homogeneous polymerization, equivalent to a single orientation within one grain, would give rise to large distortions and internal stresses. To overcome this, the deformations are localized over much smaller volumes, which in the specific case of the rhombohedral polymer results in a fine lamellar structure, with a reduced magnitude of stress, and hence a greater stability for the final state. The concentration of rhombohedral lamellae increases with treatment pressure, which concurs with the XRD studies discussed previously. Whereas the specific P–T conditions provide the thermodynamic potential for

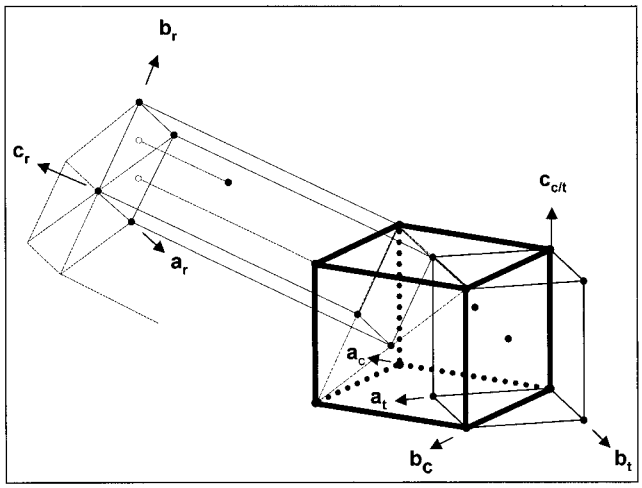

Figure 5. The relative positions and orientations of the polymer unit cells with respect to the original fcc unit cell.

the phase transformation, the kinetics may be influenced by the enhanced $(111)_C$ crystal shear with increased non-hydrostatic pressure. This shear motion could enable the C_{60} cages to align themselves in a position where the double bonds on adjacent molecules are parallel, as discussed in detail in [9]. This would facilitate a [2 + 2] cycloaddition and hence the formation of the 2-D polymer.

Structural studies in this P/T area were carried out on C_{60} by Marques *et al* [9], Blank *et al* [11, 13], Brazhkin *et al* [14, 15] and Davydov *et al* [8]; these agree with this study with respect to the production of mixed phases at lower pressures. However, at higher pressures a singular rhombohedral phase, as discovered by the previously mentioned authors, is found not to be the case in this analysis. In fact a mixed phase was discovered with a higher proportion of rhombohedral than tetragonal phase. It is therefore evident that the ratio of polymers is controlled by treatment pressure.

3.2. Graphitic 'hard' carbon

Already a considerable amount of research has been performed on this state of carbon by numerous groups worldwide [9–13], but the detail of its structure has not been established; for example, no precise explanation of its electron diffraction has been satisfactorily given. With increases in treatment temperature from 773 K, the XRD trace changes markedly, giving a broad diffuse peak with d-spacing similar to that of the (00.2) reflection of graphite. All samples synthesized at temperatures of 900 K and above behaved similarly under XRD investigation, indicating C_{60} cage collapse and the formation of graphitic carbon. The TEM images (figure 6) exhibit bands of contrast with similar frequency and orientation to those for the mixed polymeric phase. The electron diffraction pattern had three diffuse (00.2) reflections from turbostratic graphite in three layer-plane orientations corresponding to the precursor rhombohedral lamellae. Additionally, there are diffuse diffraction rings from a more disordered graphitic structure between the layered graphitic bands, agreeing with previous neutron diffraction experiments [12].

The mechanism of cage collapse could be by either of two possible routes. Firstly, the samples are exposed to vast pressures with a considerable magnitude of uniaxiality present.

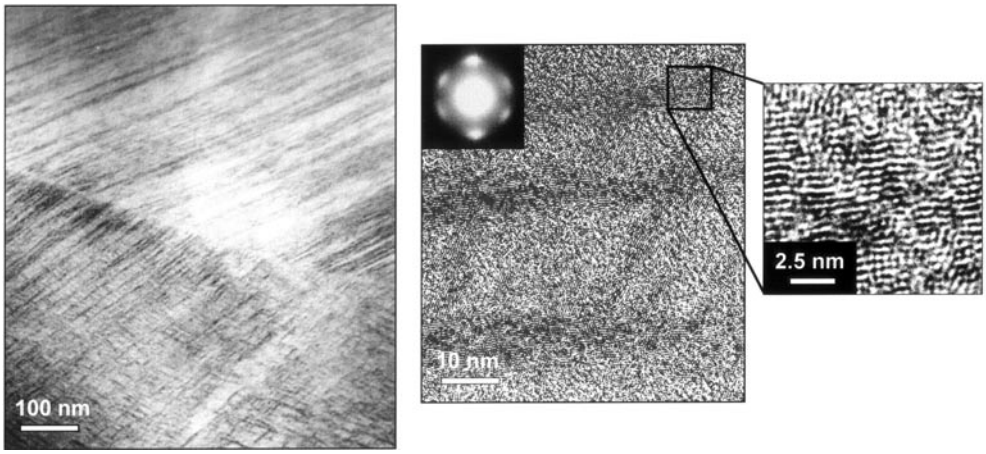

Figure 6. From left to right: a low-magnification image across an original C_{60} grain boundary and a more detailed HR-TEM of the graphitic 'hard' carbon phase.

The consequence of this is a high probability of shear occurring in the system, which could break the intermolecular bonds, initiating cage collapse. The shear bands produced by this mechanism would be parallel to $(111)_C$, which agrees with the position and orientation of the contrasting areas visible in the TEM image. Also this provides the first explanation for the graphitic structure that is truly consistent with the threefold diffuse electron diffraction pattern. The novel TEM observations, of the mixed polymeric phase, offer an alternative mechanism associated with the inherent instability of the interfacial region, in the mixed polymeric state. With an increase in temperature the molecules could acquire enough energy for bond dissociation, instigating the subsequent cage collapse.

3.3. Hardness

Initial investigations of hardness were performed on samples with heating times of one hour. Standard Vickers indentations, of the graphitized hard carbon phase, have been reported in the literature to give calculated hardness up to a value two thirds that of diamond. This is surprisingly large for a graphitic or disordered carbon phase. However, the method used to determine the hardness value is related to the magnitude of the residual indent left. This method cannot take into account the process of elastic recovery. The depth-sensing indentation techniques used in this work enabled an assessment of the true hardness to be made.

The hardness values for the graphitic phase (973 K and 1173 K, one hour) are considerably less than expected: 10–12 GPa. The large amount of elastic recovery occurring on removal of the applied load is confirmed by the load–displacement curve (figure 7), which almost reverts back to the origin during unloading.

The reason for the recovery is the ability of the corrugated graphitic layers, which have a variable spacing, to compress together without shearing, then subsequently expand back to the original structure. The physical extent of the recovery after indentation could be appreciated from the fact that the indents were too small to be located using a SEM. In contrast to this, the indentations performed on the polymeric phases were easily located due to the large quantity of plastic deformation associated with easy shear of C_{60} polymerized layers with weak, van der Waals, interlayer bonding.

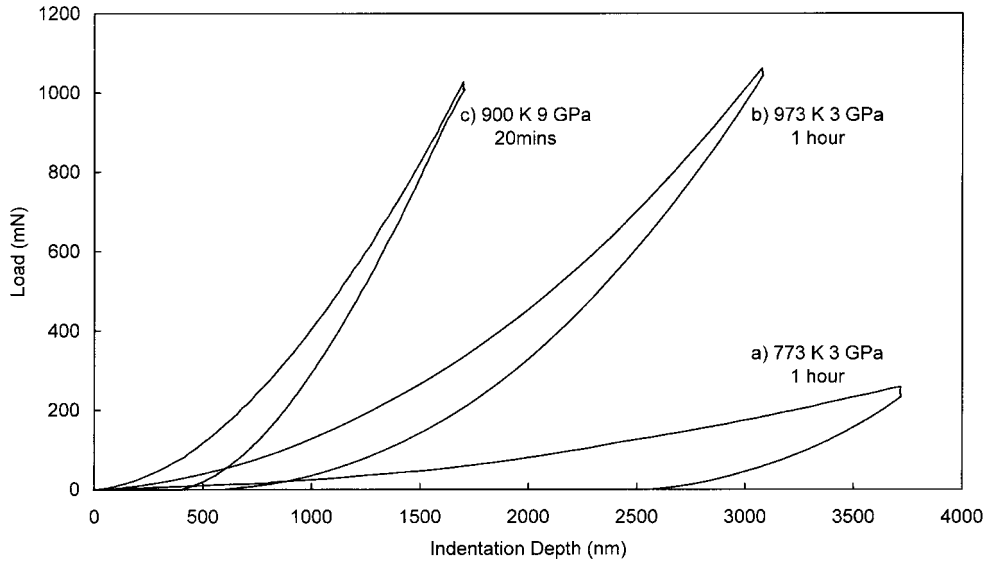

Figure 7. Load–displacement curves for the (a) polymeric, (b) graphitic and (c) 'intermediate' graphitic fullerenes.

In the bid to discover fullerenes with more advantageous hardness properties, a sequence of samples were produced at 9 GPa, over a temperature range of 700–1200 K, with shortened treatment times of one minute. Initially, it is evident that the shortened treatment time results in a considerable increase in hardness compared with that of samples treated for one hour. An overview of hardness for all of the samples tested is given in table 1. XRD investigations (figure 8) show the evolution of the polymeric phases, at 700 and 800 K, into the broad

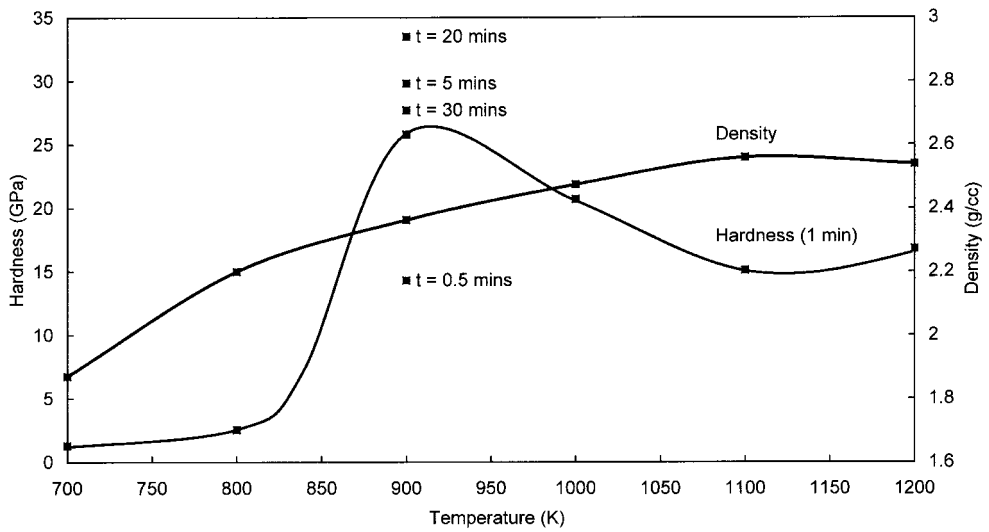

Figure 8. A hardness and density graph for samples treated at 9 GPa and various hardness values for treatment time variations at 900 K.

Table 1. Hardness values for C_{60} thermobarically treated over a range of conditions and periods.

Temperature (K)	Pressure (GPa)	Time (min)	Hardness (GPa)
773	3	60	0.7 ± 0.1
773	9	60	0.8 ± 0.1
973	3	60	11.4 ± 1.6
973	6	60	10.6 ± 1.5
973	9	60	9.8 ± 1.5
1173	3	60	10.4 ± 1.1
1173	9	60	10.3 ± 1.0
700	9	1	1.6 ± 0.1
800	9	1	2.9 ± 0.1
900	9	1	25.8 ± 1.4
1000	9	1	20.7 ± 1.2
1100	9	1	15.1 ± 0.9
1200	9	1	16.8 ± 1.5
900	9	0.5	14.3 ± 0.9
900	9	5	29.8 ± 1.3
900	9	20	33.5 ± 1.5
900	9	30	27.7 ± 1.1
Graphite	—	—	0.1
Diamond	—	—	70–130

graphitic peak at 900 K. The hardness graph (figure 9) demonstrates this as a dramatic increase in hardness from 800 to 900 K accompanied by an increase in density. The lower-temperature hardness values of 1.3 to 2.9 GPa are typical of the different states of polymerized phase. As the temperature increases, there is a rapid increase in hardness to an initial peak at 900 K of 25.8 GPa with a decrease to ∼15 GPa at 1100 and 1200 K. This variation in the hardness indicates that the formation of the graphitic phase proceeds via an intermediate state, with time-dependent structure. Therefore the relatively high hardness indicates that the intermediate state

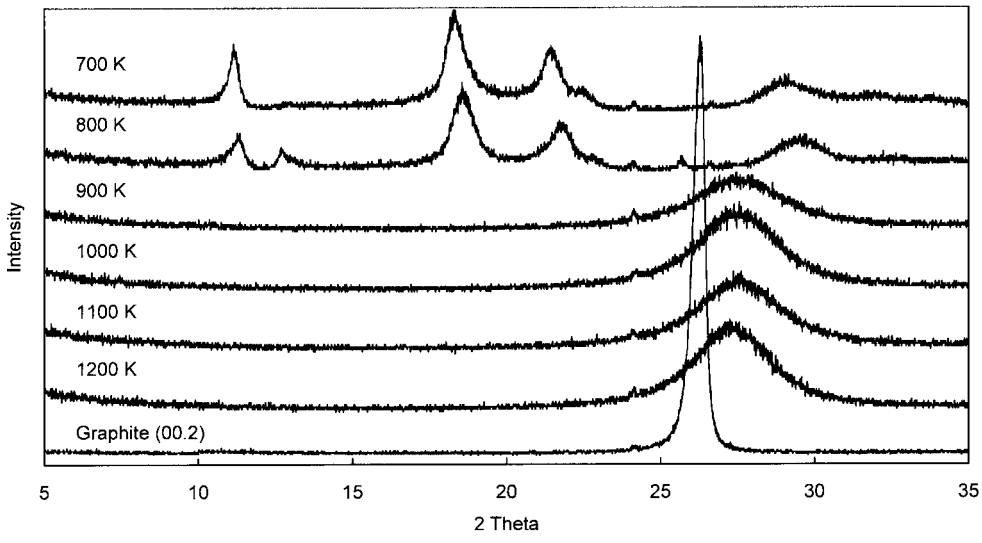

Figure 9. The evolution of XRD traces with temperature for C_{60} at a pressure of 9 GPa.

must contain a substantial quantity of remanent cross-linking between the graphitic layers. The density variation shows the expected increase with molecular cage collapse on graphitization but is, surprisingly, not sensitive to the proposed degree of cross-linking between the carbon layers. However, the time dependence of the cage collapse (which is particularly evident in the 900 K hardness data) implies that these intact molecules could become trapped between layers of the graphitic structure, hindering a reduction in d-value, and resulting in a lower density. As the treatment temperature increases, the hardness falls off, indicating a reduction in cross-linking and an increase in interlayer spacing towards that for graphite, which is evident in the XRD spectra in figure 8. However, a reduction in the density is not observed because the reduction in volume caused by the destruction of the remaining C_{60} cages dominates over the effect of an increase in d-value associated with the loss of cross-linking between the layers.

Further investigations into the effects of treatment time were undertaken at 900 K and 9 GPa, with variations from thirty seconds to thirty minutes. The sample hardness increases through times of thirty seconds, one minute, five minutes and up to a maximum of 33.5 GPa at twenty minutes. It then declines between twenty and thirty minutes and one would expect it to level off in the region of 10–15 GPa for times of one hour and over with further approach to the final graphitic state. An indication of this (figure 7) is the maximum displacement of ∼1700 nm compared with ∼3200 nm for a fully transformed graphitic state. The time/temperature influence on cage collapse and subsequent reduction in remanent cross-linking has recently been confirmed during '*in situ*' diffraction experiments within the P–T field [16]. It is notable that even after long times above 900 K the true hardness values are much greater than for a conventional graphite (typically 1 GPa for a pyrolytic turbostratic form). This indicates that interlayer shear remains inhibited both by remanent sp^3 cross-linked bonds and by the degree of localized layer corrugation and nano-scale heterogeneities in the degree of crystallinity.

4. Conclusions

At synthesis temperatures up to 773 K, 2-D alternating mixed polymeric phases are produced. TEM studies showed that at all pressures a mixed state is produced with the proportion of rhombohedral and tetragonal polymer being controlled by the treatment pressure. At lower pressures the tetragonal phase is dominant, but the rhombohedral polymer quickly becomes evident and then dominates. The alternating polymer phase is formed in an effort to reduce the stresses generated by large-volume lattice deformations, by localizing it over smaller volumes, resulting in rhombohedral lamellar domains interspersed amongst tetragonal domains.

The subsequent cage collapse during graphitization results in the formation of a graphitic 'hard' carbon phase, with mainly sp^2 bonding in regularly warped layers. The pressure uniaxiality, and hence shear, in the system and the inherent instability present at the interface of the polymer domains provide a mechanism for graphitization. Whether it is a single factor responsible for this or a combination of factors has yet to be determined. The warping of the graphitic layers results in a high degree of elastic recovery, under indentation, which explains the previously reported high hardness measured by means of residual indentation. In reality the graphitic hard carbon state has hardness in the region of 10–15 GPa. The kinetics of graphitization is slow (∼1 h) and intermediates, with whole C_{60} cages and varying degrees of cross-linking, are formed. The magnitude of cross-linking influences the properties, reaching its peak after treatment for twenty minutes, resulting in a hardness of 33.5 GPa. With the evolution of treatment time, cross-linking becomes less dominant and the interlayer spacing increases and approaches the (00.2) value of graphite.

References

[1] Kroto H W, Heath J R, O'Brien S C, Curl R F and Smalley R E 1985 *Nature* **318** 162
[2] Kratschmer W, Lamb L D, Fostiropoulos K and Huffman D R 1990 *Nature* **347** 354
[3] Rao A, Zhou P, Wang K-A, Hager G T, Holden J M, Wang Y, Lee W-T, Bi X-X, Eklund P C, Cornett D S, Duncan M A and Amster I J 1993 *Science* **259** 955
[4] Xu C H and Scuseria G E 1995 *Phys. Rev. Lett.* **74** 274
[5] Persson P-A, Edlund U, Jacobsson P, Johnels D, Soldatov A and Sundqvist B 1996 *Chem. Phys. Lett.* **258** 540
[6] Sundqvist B, Edlund U, Jacobsson P, Johnels D, Jun J, Launois P, Moret R, Persson P-A, Soldatov A and Wagberg T 1998 *Carbon* **36** 657
[7] Rao A M, Eklund P C, Venkateswaran U D, Tucker J, Duncan M A, Bendele G M, Stephens P W, Hodeau J-L, Marques L, Nunez-Regueiro M, Bashkin I O, Ponyatovsky E G and Morovsky A P 1997 *Appl. Phys.* A **64** 231
[8] Davydov V A, Kashevarova L S, Rakhmanina A V, Agafonov V, Allouchi H, Ceolin R, Dzyabchenko A V, Senyavin V M and Szwarc H 1998 *Phys. Rev.* B **58** 14 786
[9] Marques L, Hodeau J-L, Nunez-Regueiro M and Perroux M 1996 *Phys. Rev.* B **54** 12 633
[10] Kozlov M E, Tokumoto M and Yakushi K 1997 *Appl. Phys.* A **64** 241
[11] Blank V D, Denisov D N, Ivlev A N, Mavrin B N, Serebryanaya N R, Dubitsky G A, Sulyanov S N, Popov M Y, Lvova N A, Buga S G and Kremkova G N 1998 *Carbon* **36** 1263
[12] Bennington S M, Kitamura N, Cain M G, Lewis M H and Arai M 1999 *Physica* B **263+264** 632
[13] Blank V D, Buga S G, Serebryanaya N R, Dubitsky G A, Popov M Y and Sundqvist B 1998 *Carbon* **36** 319
[14] Brazhkin V V, Lyapin A G and Popova S V 1996 *JETP Lett.* **64** 755
[15] Brazhkin V V, Lyapin A G, Popova S V, Voloshin R N, Antonov Yu V, Lyapin S G, Kluev Yu A, Naletov A M and Mel'nik N N 1997 *Phys. Rev.* B **56** 11 465
[16] Bennington S M, Kitamura N, Cain M G, Lewis M H, Wood R A, Fukumi K and Funakoshi K 2000 *J. Phys.: Condens. Matter* **12** L451